Considerations for the design of bottom intake systems

José M. Carrillo, Luis G. Castillo, Juan T. García and Álvaro Sordo-Ward

ABSTRACT

Knowing the scarcity of water in the southeast of Spain and how the rain occurs, we considered the design of intake systems in ephemeral riverbeds in order to try to capture part of the runoff flow. The intake systems generally consist of a rack located in the bottom of a river channel, so that the water collected passes down the rack and leads to the side channel. This behaviour has been studied in the laboratory by several researchers. However, due to the many effects that occur on the bars, it is not possible to analyse the whole problem of characterization with traditional methodologies. For instance, the wetted rack length necessary to collect a required flow presents important differences depending on what each author has considered relevant. Computational fluid dynamics simulations have been done to improve the knowledge of the hydraulic phenomenon observed in different laboratory experiences, for which we have previously calibrated the numerical models using laboratory results. The ANSYS CFX code was selected. Several two-equation turbulence models have been considered. The results show differences smaller than 1% in the wetted rack length, and discharge coefficients also present good agreement.

Key words | ANSYS CFX, bottom intake system, bottom rack, discharge coefficient, street gully, turbulence models

José M. Carrillo (corresponding author)
Luis G. Castillo
Juan T. García
Civil Engineering Department,
Universidad Politécnica de Cartagena, UPCT,
Paseo Alfonso XIII, 52, 30203 Cartagena,
Spain
E-mail: *jose.carrillo@upct.es*

Álvaro Sordo-Ward
Civil Engineering Department,
Universidad Politécnica de Madrid, UPM,
Campus Moncloa, 28040 Madrid,
Spain

INTRODUCTION

Intake systems generally consist of a rack located in the bottom of the channel that allows water to pass through. These structures have been adopted in small mountain rivers with steep slopes and an irregular riverbed, intense sediment transport and flash flood. Their design is intended to satisfy two primary objectives: (1) to maximize water intake; and (2) to minimize sediment intake.

In designing intake systems, we need to consider geomorphologic, hydraulic, structural and economic aspects to avoid unnecessary maintenance and functionality problems during the lifetime of the project. The efficiency of racks depends on a number of factors, such as the number of bars, incoming flow conditions, longitudinal inclination, shape and spacing between bars.

The hydraulic behaviour of the racks is also influenced by the bars' disposition. In longitudinal bars, the flow collected appears as a function of the local energy flow. However, in transversal bars or circular perforations, the flow collected is related to the local flow level (Mostkow 1957).

In the analysis of clear water flows it is assumed that the flux over the rack is one-dimensional, the flow decreases progressively, and the hydrostatic pressure distribution acts over the rack in the flow direction. Two broad approaches to dealing with the energy head over the rack are typically used and these are presented in Table 1.

The classical approach considers a two-dimensional perspective. However, when analyzing the flow near the solid edges, the flow becomes extremely three-dimensional, rendering the two-dimensional analysis tools less useful.

In numerical modelling, different approaches have been used. Some codes, such as HEC-RAS, MIKE, TELEMAC or

doi: 10.2166/hydro.2017.008

Table 1 | Simplification of the energy head along the rack

Horizontal energy level	Energy level parallel to the rack plane
Kuntzmann & Bouvard (1954), Frank & Von Obering (1956), Free overfall (Henderson 1966), Vargas (1998), Drobir *et al.* (1999), Brunella *et al.* (2003) and Righetti & Lanzoni (2008)	Chaguinov (1937), Noseda (1956a, 1956b), Gherardelli (1956), Mostkow (1957), Dagan (1963) and Krochin (1978)

IBER, consider one-dimensional and two-dimensional models to study the hydraulic behaviour of rivers and sediment transport phenomena (Castillo *et al.* 2015; USACE 2016). Nevertheless, flows occurring in hydraulic structures tend to be highly three-dimensional (Bayon *et al.* 2016; Castillo *et al.* 2016). For this reason, three-dimensional models were considered in this study.

The rest of this paper is organized as follows. The Purpose section indicates the challenges and objectives of the study. The Theoretical background section is a literature review to familiarize the reader with the empirical expressions obtained by several authors to calculate intake systems. The Methods section introduces the main characteristics of the laboratory equipment and of the numerical simulations carried out. The Results section compares the laboratory and simulated data in terms of mesh size sensitivity, turbulence models, flow profiles over the rack, wetted rack length, water collected and discharge coefficient. The Discussion section explains the main findings related to the purpose of the study. Finally, the Conclusions section briefly summarizes the overall conclusions of the work.

PURPOSE

As a result of the lack of water resources in several parts of the world, bottom intake systems are a point of great interest. Research to date has been developed in the laboratory. Thanks to the computational fluid dynamics (CFD) programs, researchers and designers can evaluate different effects with a smaller cost than that incurred by building scale models. However, references to numerical simulations of bottom intake systems are scarce.

As a result of the lack of numerical simulations in this field, the present paper is focused on filling the gap between laboratory results and CFD simulations in T-shape bottom racks. ANSYS CFX software (version 16.2) is used to analyse the flow profiles over the rack, and the collected water along the intake system. Due to the variety of turbulence models, and in order to compare their effect over different parameters, three distinct two-equation turbulence models are examined.

Knowing the parameters analysed, designers will be able to design the bottom intake system with greater certainty.

THEORETICAL BACKGROUND

Wetted rack length

Several researchers have estimated the theoretical wetted rack length L necessary to derive a defined flow rate q_1. The different required lengths are due to the variation of experimental conditions used to adjust the discharge coefficient, such as the shape of the bars, their separation and width, the void ratio, the approximation flow conditions, the initial flow depth h_1 or the longitudinal rack slope θ.

Figure 1 differentiates the wetted rack length in two magnitudes: the distance along the rack where the nappe enters directly through the racks (measured between the bars), called L_1, and the maximum distance where the bars are wet, called L_2.

The theoretical longitudinal rack slope, θ, has been considered in several ways. Some authors consider the influence of the slope in the required wetted rack length (Garot 1939; Orth *et al.* 1954; White *et al.* 1972; Righetti & Lanzoni 2008). Other researchers experimentally found that there is no further influence for slopes greater than 19° (34.43%) (Brunella *et al.* 2003).

Castillo & Lima (2010) and García (2016) compared the wetted rack length proposed by several authors, for the case of critical conditions at the beginning of the rack, void ratio $m = 0.60$, and longitudinal rack slope of 20% (Figure 2). In each case, the horizontal energy level remains constant along the rack. Differences may be double in some cases.

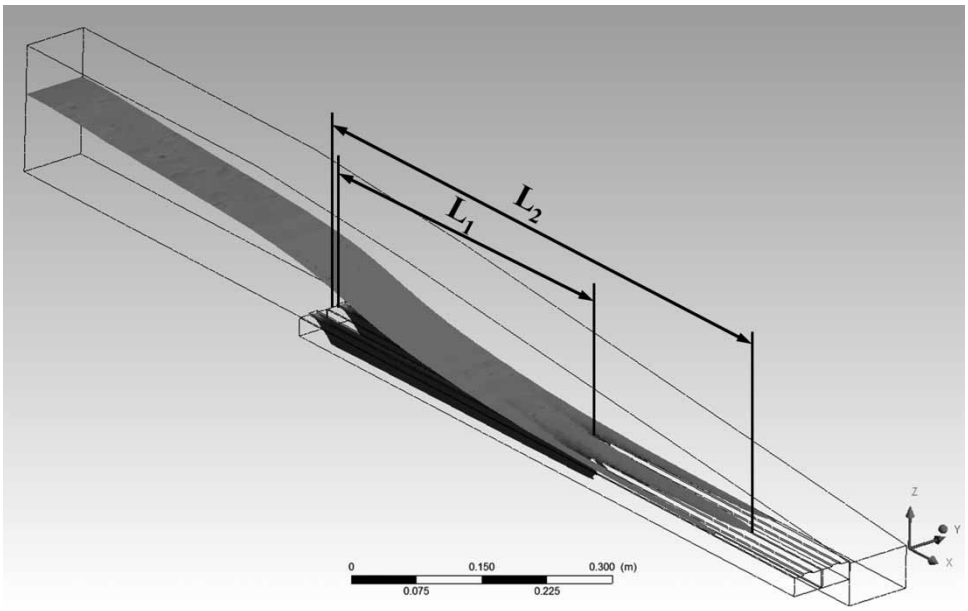

Figure 1 | Scheme of wetted rack lengths L_1 and L_2.

In Figure 2, the length proposed by Righetti & Lanzoni (2008) approaches the free overfall (Henderson 1966). These authors introduced the approximation level conditions in their formula and critical approximation conditions were adopted. These differ from other experimental results. There are also some field measurements in a prototype made with circular bars (Drobir *et al.* 1999).

To avoid rack occlusion, several authors proposed design recommendations from prototype observations in mountain rivers (e.g., Orth *et al.* 1954; Ract-Madoux *et al.* 1955; Krochin 1978; Drobir 1981; Bouvard 1992; Raudkivi

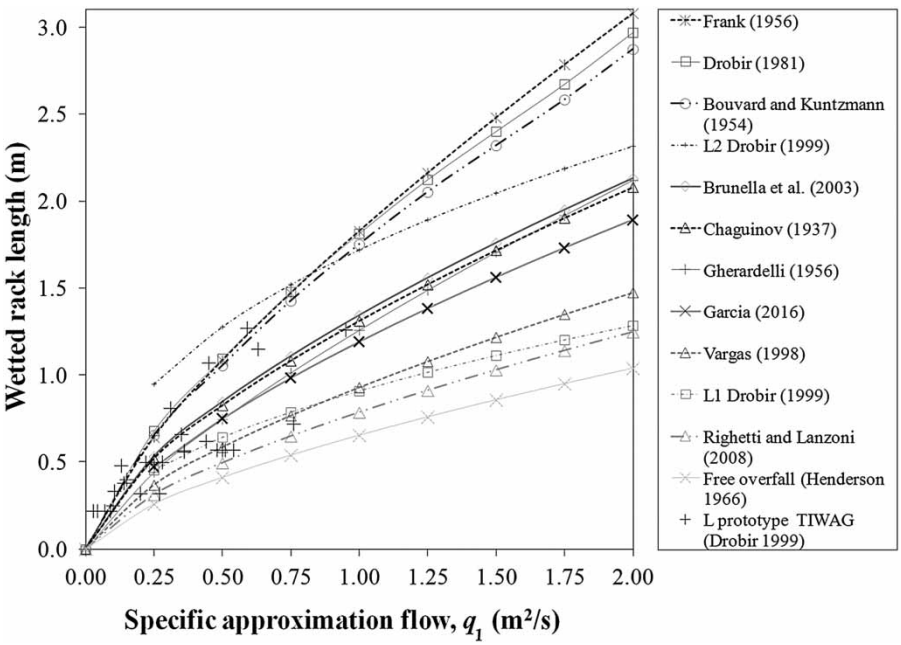

Figure 2 | Review of wetted rack lengths for racks with void ratio $m = 0.60$ and 20% of slope (adapted from Castillo & Lima 2010; García 2016).

1993). Castillo *et al.* (2016), from experimental measurements in a flow with gravel-sized materials, determined that a longitudinal rack slope around 30% minimizes the occlusion effect.

Discharge coefficient

The specific derived flow through the bottom rack per unit of length and width, $q_d = dq/dx$ ($m^3/s/m$), may be calculated using the orifice equation. The collected flow through the rack plane is influenced by the velocity distribution close to it. The deviation from the uniform distribution is included in the velocity coefficient, C_v. In a similar way, there is a change in the available section, which involves the flow contraction. In this case, a contraction coefficient, C_c, may be considered. Both coefficients require experimental measurement and depend on the shape of the bars and the spacing between them. The orifice equation may be written as:

$$\frac{dq}{dx} = C_v C_c m\sqrt{2gH} = C_{qH} m\sqrt{2gH} \quad (1)$$

where m represents the relation void area and the total area (void ratio), H the total energy available refers to the plane of the rack, x the longitudinal coordinate along the rack, and C_{qH} the discharge coefficient depending on the energy height ($C_{qH} = C_c C_v$).

In some cases, the specific derived flow may be obtained as a function of the water depth along the rack, h. Hence, the orifice equation is:

$$\frac{dq}{dx} = C_{qh} m\sqrt{2gh} \quad (2)$$

where C_{qh} is the discharge coefficient as a function of the water depth normal to the rack plane.

Table 2 shows the discharge equation, considered by several authors.

Righetti *et al.* (2000) considered that it is possible to calculate the differential flow of the water collected as:

$$dq(x) = C_{qH} m\sqrt{2g(H_0 + \Delta z)}dx \quad (3)$$

where m is the void ratio, dx the increment longitudinal in the flow direction, H_0 the specific energy at the beginning of the rack, Δz the vertical difference between the initial rack section and the analysed section, and C_{qH} is the discharge coefficient.

The same authors proposed that $C_{qH} \approx \sin\theta$, with θ being the angle between the velocity vector of water derived and the plane of the rack (Figure 3).

Table 2 | Expressions to calculate the discharge flow through longitudinal racks

Author	dq/dx
Garot (1939)	$C_{qh} m\sqrt{2gh(x)}$
De Marchi (1947)	$C_{qH} m\sqrt{2gH_0}$
Bouvard (1953)	$C_{q0} m\sqrt{2gh(x)\cos\theta}$
Noseda (1956a, 1956b)	$C_{qh}(h) m\sqrt{2gh(x)}$
Frank & Von Obering (1956)	$C_{qh} m\sqrt{2gh(x)\cos\theta}$
Mostkow (1957)	$C_{qH} m\sqrt{2gH_0}$
Nakagawa (1969)	$C_{qH}(x) m\sqrt{2gH_0}$
Krochin (1978)	$C_{qH} m\sqrt{2gH_0}$
Brunella *et al.* (2003)	$C_{q0} m\sqrt{2gh(x)\cos\theta}$
Ahmad & Mittal (2003), Ghosh & Ahmad (2006) and Kumar *et al.* (2010)	$C_{qH} m\sqrt{2gH_0}$
Righetti & Lanzoni (2008)	$C_{qH}(x) m\sqrt{2gH_0}$

Note: h(x) is the normal water surface height depending on the *x* coordinate, $C_{qh}(x)$ the discharge coefficient depending on *h*, $C_{qH}(x)$ the discharge coefficient depending on the energy and the *x* coordinate, H_0 the energy height at the beginning of the rack, C_{q0} the discharge coefficient measured under static conditions (with negligible approaching velocity), and θ the angle of the rack with the horizontal.

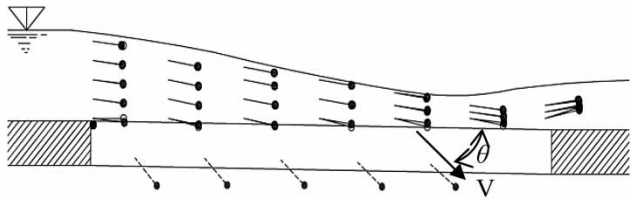

Figure 3 | Inclination θ of the streamlines of the flow collected (Righetti *et al.* 2000).

Flow profile over the rack

The flow profile over the rack has also been analysed by several authors (Table 3).

With velocity measurements in the free surface, Brunella *et al.* (2003) found that the dissipation effects are insignificant. However, in the final part of the racks these effects cannot be neglected since the local effects generate friction effects. Differences between measured and calculated depth profiles at the beginning of the

Table 3 | Expressions to calculate the flow profile over the rack

Author	Flow profile over the rack (*dh/dx*)
Garot (1939)	$\frac{dh}{dx} = -2mC_{qh}\frac{\sqrt{h(H-h)}}{2H-3h}$
De Marchi (1947)	$\frac{dh}{dx} = k\frac{h(-(\partial q/\partial x))q}{gh^3-q^2}$
Noseda (1956a, 1956b)	$\Phi\left(\frac{h}{H}\right) = \frac{H}{mC_{qh}}\left[\frac{1}{2}\arccos\sqrt{\frac{h}{H}} - \frac{3}{2}\sqrt{\frac{h}{H}\left(1-\frac{h}{H}\right)}\right]$
Frank & Von Obering (1956)	$\frac{\bar{s}^2}{L^2} + \frac{(h-h_0)^2}{h_0^2} = 1; x = \frac{\bar{s}}{L}; y = \frac{h}{h_0}$
Dagan (1963)	$h.\sqrt{\frac{1-h}{1+(dh/dx)^2}} = h_0.\sqrt{1-h_0}(1-q)$
García (2016)	$\frac{dh}{dx} = \frac{2mC_{qH}\sqrt{(H_0+x\sin\theta)(H_0+x\sin\theta-h\cos\theta)}+h\sin\theta}{3h\cos\theta-2(H_0+x\sin o\theta)}$
García (2016)	$\frac{dh}{dx} = \frac{2mC_{qh}(h)\sqrt{h\cos\theta(H_0-h\cos\theta)}}{3h\cos\theta-2(H_0)}$

rack are due to the consideration of hydrostatic pressure distribution.

METHODS

Physical device

An intake system based on the physical model analysed by Noseda (1956a, 1956b) was built in the Hydraulic Laboratory of the Universidad Politécnica de Cartagena (Figure 4). It consists of a 5.00 m long and 0.50 m wide approximation channel, a rack with different slopes (from horizontal to 33%), the discharge channel, and the collected discharge water channel. The model was made with methacrylate walls allowing for direct observation of the flow.

The racks were located at the bottom of the channel. They were built with aluminium bars with T profiles (T 30/25/2 mm) with the spacing parallel to the direction of the flow. The bars used had the same width, but the longitudinal layout was modified to consider different spacing between them.

The rack was 0.90 m in length. The spacing between bars was 11.70 mm. With those considerations, the void fraction analysed was $m = 0.28$. The inlet flow rates were measured by an electromagnetic flowmeter Endress Häuser Promag 53 W of 125 mm with an error of 0.5% of the full scale. The rejected flow rates were measured by a 90 V-notch weir. The collected or derived flows were obtained as the difference between them. Once steady conditions were reached, a vertical point gauge with an accuracy of 0.5 mm was used to measure the free surface flow profile. Further details on the experimental setup can be found in Castillo *et al.* (2017b).

The inflow was subcritical in all the cases at the beginning of the inlet channel. The flow reached supercritical conditions at the beginning of the rack. In each experiment, the inlet and exit flows and the longitudinal flow profile were measured. q_1 is the entrained specific flow, while q_2 is the specific discharge flow, and q_d is the specific discharge flow collected in the intake system.

Numerical modelling

CFD programs allow for the simulation of the interaction among different fluids as a two-phase air-water flow, or flows with different concentrations in the case of sediment transport. The programs solve the fluid mechanic problem in various geometric configurations, providing a great deal of data, with greater flexibility and speed than that obtained with experimental procedures. However, mathematical models still present accuracy issues when modelling some hydraulic phenomena (Chanson & Gualtieri 2008). For correct use, it is necessary to contrast and to calibrate with data obtained in prototypes or physical models.

Figure 4 | Intake system physical device.

To test the hydraulic behaviour of the intake system, laboratory measurements were used to model and calibrate CFD simulations. The Finite Volume Scheme program ANSYS CFX (version 16.2) has been used. This program was previously used for solving intake systems with accurate results (Castillo *et al.* 2014b).

For turbulent flow, CFD codes solve the differential Reynolds-averaged Navier–Stokes (RANS) equations of the phenomenon in the fluid domain, retaining the reference quantity (mass, momentum, energy) in the three directions for each control volume identified. The equations for conservation of mass and momentum may be written as:

$$\frac{\partial \rho}{\partial t} + \frac{\partial}{\partial x_j}\left(\rho U_j\right) = 0 \tag{4}$$

$$\frac{\partial \rho U_i}{\partial t} + \frac{\partial}{\partial x_j}\left(\rho U_i U_j\right) = -\frac{\partial p}{\partial x_i} + \frac{\partial}{\partial x_j}\left(2\mu S_{ij} - \rho\overline{u_i' u_j'}\right) \tag{5}$$

where i and j are indices, x_i represents the coordinates directions ($i = 1$ to 3 for x, y, z directions, respectively), ρ the flow density, t the time, U the velocity vector, p the pressure, u_i' presents the turbulent velocity in each direction ($i = 1$ to 3 for x, y, z directions, respectively), μ is the molecular viscosity, S_{ij} is the mean strain-rate tensor and $-\rho\overline{u'_i u'_j}$ is the Reynolds stress.

Although the RANS equations can be applied to variable-density flows, in this case Navier–Stokes equations are considered in their incompressible form.

Turbulence models

To reach closure of the Navier–Stoke equations, one-equation to direct simulation turbulence models can be used.

As a compromise between accuracy and computational effort, the RANS turbulence models are widely used. Eddy viscosity turbulence models consider that such turbulence consists of small eddies which are continuously forming and dissipating, and in which the Reynolds stresses are assumed to be proportional to mean velocity gradients. The Reynolds stresses may be related to the mean velocity gradients and eddy viscosity by the gradient diffusion hypothesis:

$$-\rho\overline{u_i'u_j'} = \mu_t\left(\frac{\partial U_i}{\partial x_j}+\frac{\partial U_j}{\partial x_i}\right)-\frac{2}{3}\delta_{ij}\left(\rho k+\mu_t\frac{\partial U_k}{\partial x_k}\right) \quad (6)$$

with μ_t being the eddy viscosity or turbulent viscosity, $k = 1/2\overline{u'_i u'_i}$ the turbulent kinetic energy and δ the Kronecker delta function.

The choice of the turbulence model may have great importance in some studies (Castillo & Carrillo 2017). In this work, some of the most usual RANS turbulence models have been tested.

Standard k-ε model

This model (Launder & Sharma 1972) is considered as the standard turbulence model and it is considered in the majority of the CFD programs. The effective viscosity is calculated as:

$$\mu_t = C_\mu\rho\frac{\kappa^2}{\varepsilon} \quad (7)$$

where C_μ is an empirical coefficient and ε is the dissipation rate of turbulent kinetic energy.

Re-normalization group k-ε model

In theory, the re-normalization group (RNG) k-ε model is more accurate than the standard k-ε model. The RNG k-ε turbulence model is based on a RNG analysis of the Navier–Stokes equations. The transport equations for turbulence generation and dissipation are the same as those for the standard model, although the model constants differ and the constant $C_{\varepsilon 1}$ is replaced by the function $C_{\varepsilon 1RNG}$ (Yakhot & Smith 1992):

$$C_{\varepsilon 1RNG} = 1.42 - f_\eta \quad (8)$$

with this being:

$$f_\eta = \frac{\eta(1-(\eta/4.38))}{(1+\beta_{RNG}\eta^3)}, \quad \eta = \sqrt{\frac{P_\kappa}{\rho C_{\mu RNG}\varepsilon}} \quad (9)$$

where $C_{\mu RNG} = 0.085$ is a closure coefficient, β_{RNG} a constant with a value of 0.012, P_k the turbulence production due to viscous forces (ANSYS Inc. 2015), ρ the flow density and ϵ the dissipation rate of turbulent kinetic energy.

k-ω based shear-stress transport model

The k-ω turbulence models assume that the turbulence viscosity is linked to the turbulence kinetic energy, k, and the turbulent frequency, ω, as:

$$\mu_t = \rho\frac{\kappa}{\omega} \quad (10)$$

The shear-stress transport (SST) model takes into account the accuracy of the k-ω model in the near wall region and the free stream independence of the k-ε model in the outer part of the boundary layer. To do this, the original k-ω model (Wilcox 2006) is multiplied by a blending function F_1, while the k-ε model (Launder & Sharma 1972) is transformed to a k-ω formulation and multiplied by a function $1-F_1$ (Menter 1994). F_1 is designed to be 1 inside the boundary layer and decreases to a value of 0 away from the surface. If Φ_1 represents any constant in the original k-ω model and Φ_2 represents any constant in the transformed k-ε model, then the corresponding constant in the model Φ_3 may be written as:

$$\Phi_3 = F_1\Phi_1 + (1-F_1)\Phi_2 \quad (11)$$

From the three two-equation turbulence models considered, this model has obtained the best results in the study of free surface falling jets (see Castillo *et al.* 2014a, 2017a).

Convergence criteria

In judging the convergence of a solution in a finite volume scheme, a widely used method entails monitoring the

residuals. Residuals are defined as the imbalance in each conservation equation following each iteration. The solution is said to have converged if the scaled residuals are smaller than prefixed values ranging between 10^{-3} and 10^{-6}. In this work, the residual values were set to 10^{-4} for all the variables.

Free surface modelling

To solve the air-water two-phase flow, the Eulerian–Eulerian multiphase flow homogeneous model was selected. In each control volume, the sum of volume fraction of all phases (r_α) is the unit. Three conditions are possible for each cell:

- $r_\alpha = 0$. The cell is empty of the α phase.
- $r_\alpha = 1$. The cell is full of the α phase.
- $0 < r_\alpha < 1$. The cell contains the interface between the α phase and one or more other phases.

It may be assumed that the free surface is on the 0.5 air volume fraction.

Boundary conditions

The model boundary conditions corresponded to the flow, the turbulence at the inlet condition obtained with an acoustic Doppler velocimeter (located 0.50 m upstream of the front edge of the rack), the upstream and downstream water levels, and their hydrostatic pressure distributions. In the bottom of the exit channel of water collected, opening boundary conditions were used. For simplicity, it was considered that all the longitudinal bars work in the same mode in the intake system. For this reason, the domain fluid considers three bars and two spaces between bars. Symmetry conditions were used in the central plane of the extreme bars (Figure 5).

For the walls and the rack, no slip wall conditions and smooth walls were considered. The atmospheric condition was simulated as an opening condition with a relative pressure of 0 Pa, air volume fraction of 1 and water volume fraction of 0.

RESULTS

Before studying all the range of flows and slopes in the intake system, mesh sensitivity analysis and turbulence model comparisons were performed. Once the best options were obtained, the different settings of the physical model were analysed. Laboratory and simulated data were compared at the same geometric scale after the steady state was reached.

Mesh size independence

In the study of intake systems, there is flow separation and high turbulence that need high quality mesh elements to

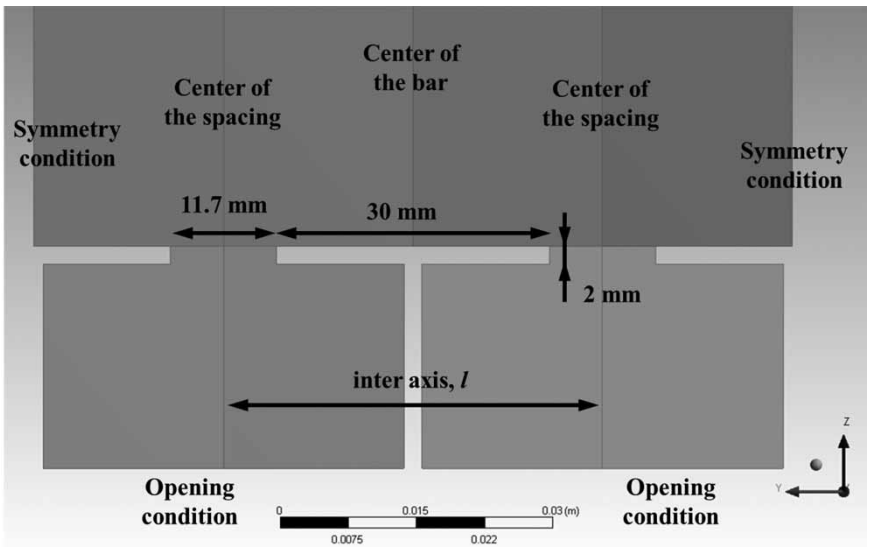

Figure 5 | Detail of the domain fluid near the rack.

solve the problem with the highest accuracy. For these reasons, hexahedral mesh elements were used.

To determine the accuracy of the numerical simulations data, in the first place, the flow profiles along the rack were compared by using three different mesh sizes (0.002, 0.004 and 0.008 m). Table 4 shows the number of elements and the mean time required to solve the simulations using an 8-core Intel(R) Xeon(R) CPU at 2.40 GHz and with 12 GB of RAM.

Figure 6 compares the flow profiles measured in the laboratory over the centre of the bars with the simulated data obtained for the three mesh sizes considered. Table 5 shows the comparison of water depths for the $q_1 = 155.4$ l/s/m. In all the cases, the water profiles obtained with the CDF methodology were similar to the laboratory measurements (differences smaller than 0.70% of the characteristic length over bars, L_2, for the 0.004 and 0.002 m mesh sizes and smaller than 1.30% for the 0.008 m mesh size). The water depths obtained with the 0.008 m mesh size tend to be slightly smaller than the measurements and the other mesh sizes. This seems to be related to the way in which CFX obtains the interface capture approach of the free surface (ANSYS Inc. 2015). When the mesh sizes increases, the precision of the interface tends to be smaller. There are no outstanding differences between the results obtained with the 0.004 and 0.002 m mesh sizes.

As there are no remarkable differences between the results obtained with the intermediate and the smaller mesh size, but the required time is around five times longer with the 0.002 m mesh size, the 0.004 m mesh size was used to analyse the different specific flows and rack slopes.

Table 4 | Number of elements and solver mean required time as a function of the mesh size

Mesh size (m)	Number of elements	Mean required time
0.002	2,501,741	22 h
0.004	313,342	4 h
0.008	51,393	2 h

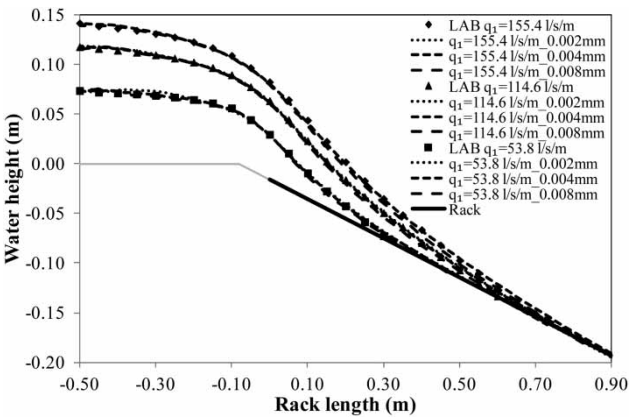

Figure 6 | Flow profiles over the centre of the bar with 20% rack slope as a function of the mesh size.

Table 5 | Water depths over the centre of the bar in different sections of the rack for the $q_1 = 155.4$ l/s/m and 20% rack slope

Rack section (m)	Water depth (m)			
	Laboratory	Mesh = 0.002 m	Mesh = 0.004 m	Mesh = 0.008 m
−0.50	0.142	0.142	0.142	0.142
0.00	0.097	0.095	0.095	0.094
0.15	0.070	0.066	0.066	0.060
0.30	0.045	0.039	0.039	0.035
0.45	0.029	0.024	0.023	0.017
0.60	0.018	0.014	0.013	0.005
0.75	0.009	0.007	0.007	0.002
0.90	0.002	0.002	0.002	0.000

Turbulence model

The influence of the turbulence model has also been analysed. Three different turbulence models have been considered: the standard k-ε, the RNG k-ε, and the SST models.

Figure 7 compares the flow profiles over the centre of the bars, measured and simulated. For the cases considered, there are no remarkable differences between the three turbulence models.

Although there are no outstanding differences, the SST turbulence model was selected to analyse the different specific flows and rack slopes, based on previous studies comparing the three turbulence models in free falling flows (Castillo *et al.* 2014a, 2017a).

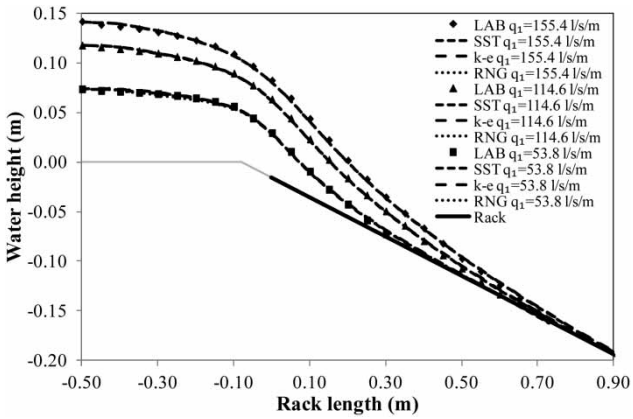

Figure 7 | Flow profiles over the centre of the bar with 20% rack slope as a function of the turbulence model.

Flow profiles over the rack

Once the mesh size and the turbulence model had been tested, simulations were carried out with five specific flows and five slopes.

In order to know the accuracy of the numerical simulations data, the longitudinal flow profiles calculated with CFD were compared with the experimental measurements in the laboratory. Figures 8 and 9 show the longitudinal flow profiles over the rack for three specific flows (77.0, 114.6 and 155.4 l/s/m), measured and simulated over the centre of the bars. In both cases, the values show a good agreement.

Wetted rack length

Knowing the required length of the rack necessary to derive a determinate flow is essential for the designers.

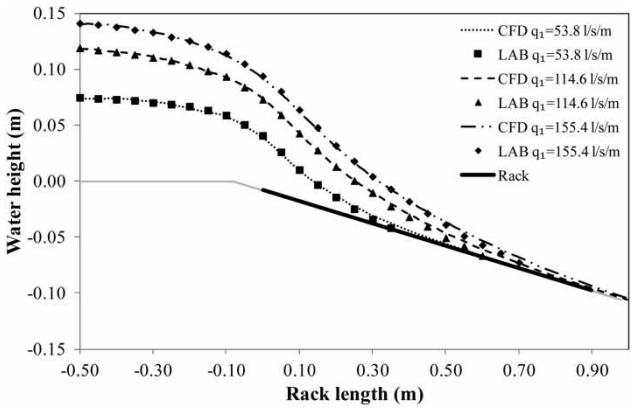

Figure 8 | Flow profiles over a bar for a rack slope of 10%.

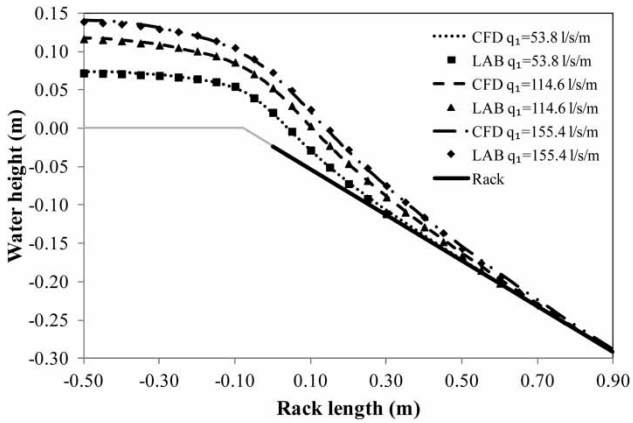

Figure 9 | Flow profiles over a bar for a rack slope of 30%.

Experimental measurements and CFD simulated values of L_1 and L_2 have been used to compare the required rack length for several specific flows and slopes (Tables 6 and 7). Differences between measured and calculated rack lengths are around 1% of the laboratory value for all the cases considered. Those differences tend to increase as the input discharge decreases. This seems to be related to

Table 6 | Comparison of L_1 and L_2 for the rack slope = 10%

Rack slope = 10%

q_1 (l/s/m)	L_{1_lab} (m)	L_{2_lab} (m)	L_{1_CFD} (m)	L_{2_CFD} (m)	Error L_1 (%)	Error L_2 (%)
155.4	0.812	>0.90	0.808	>0.90	0.485	–
138.88	0.744	>0.90	0.740	>0.90	0.532	–
114.6	0.636	>0.90	0.633	>0.90	0.609	–
77.00	0.457	0.839	0.453	0.835	0.849	0.473
53.8	0.334	0.664	0.330	0.660	1.183	0.598

Table 7 | Comparison of L_1 and L_2 for the rack slope = 30%

Rack slope = 30%

q_1 (l/s/m)	L_{1_lab} (m)	L_{2_lab} (m)	L_{1_CFD} (m)	L_{2_CFD} (m)	Error L_1 (%)	Error L_2 (%)
155.4	0.711	0.781	0.707	0.777	0.520	0.485
138.88	0.653	0.731	0.650	0.727	0.577	0.521
114.6	0.569	0.646	0.565	0.643	0.664	0.589
77.00	0.408	0.512	0.404	0.508	0.918	0.741
53.8	0.292	0.397	0.289	0.393	1.065	0.954

the associated reduction of the water depth, more accurate results being obtained with higher water depth situations.

Water collected

Figures 10 and 11 compare the water collected along the rack length for several specific flows and two different rack slopes. In both cases, the ratio flow entrained–flow collected is almost the same. In the laboratory, it was only possible to measure in the first 50 cm of the rack length and the total water collected flow. After this distance, the water flows were very small and it was therefore complicated to split the increments in the collected and the rejected flows. As a result of the shape of the T bars, the surface tension phenomena tend to cause high values of L_2, even when more than 95% of q_1 is derived in the vicinity of L_1.

Discharge coefficient

Following the idea proposed by Righetti & Lanzoni (2008), the angle of the velocity vector of water collected with the rack plane, θ, has been obtained in the numerical simulations as an estimator of the discharge coefficient along the rack. Figures 12 and 13 compare the results obtained for different specific flows and rack slopes. The numerical results have been compared with the empirical expression proposed by García (2016) for T shape bars:

$$C_{qH} \approx \frac{0.58e^{-0.75((x/h_c)m)}}{1+0.9tan\theta} \tag{12}$$

Equation (12) was adjusted by using experimental measurements of the derived flow in Equation (3). The hypothesis of $H_0 = H_{min}$ for the incoming flow was adopted for this adjustment. The discharge coefficient proposed in

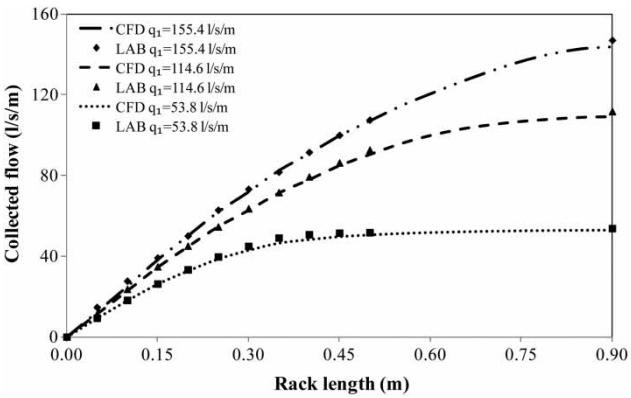

Figure 10 | Derivation capacity of the intake system with rack slope = 10%.

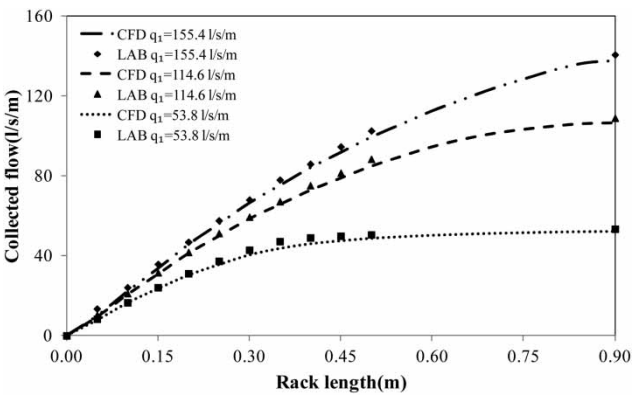

Figure 11 | Derivation capacity of the intake system with rack slope = 30%.

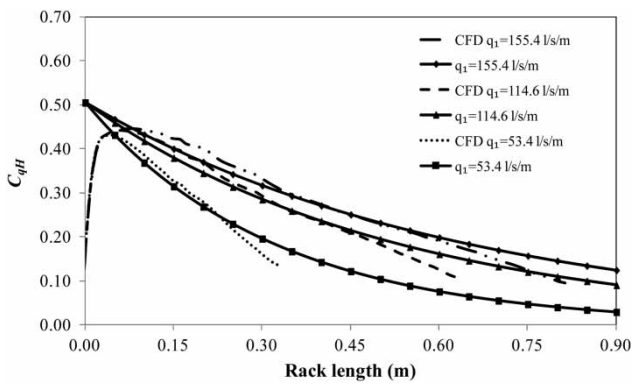

Figure 12 | Comparison of the discharge coefficient along the rack for a rack slope of 10%.

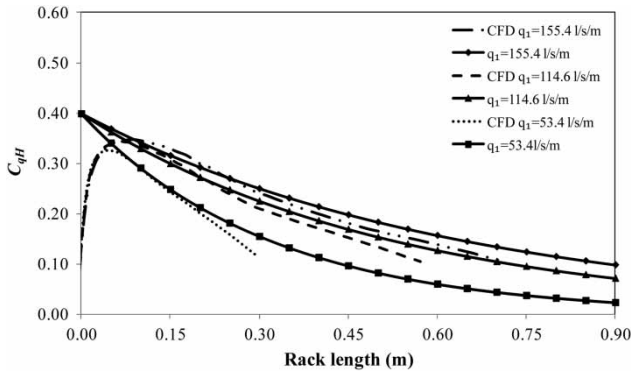

Figure 13 | Comparison of the discharge coefficient along the rack for a rack slope of 30%.

Table 8 | Ratio between the energy head and the minimum energy head at the beginning of the rack

tan θ	H_{min}/H_0
0.1	0.902
0.3	0.762

Equation (12) avoids the requirement of the water depth along the rack to calculate the derived flow.

Table 8 shows the differences between the energy head measurements at the beginning of the rack, H_0, and the minimum energy, H_{min}. To obtain the empirical discharge coefficient related to the real energy head, Equation (12) has been multiplied by the square root of the ratio H_{min}/H_0.

Despite the fact that we have used different bars types, and flow conditions from Righetti & Lanzoni (2008), similar results are obtained in terms of verifying $C_{qH} \approx \sin\theta$. At the beginning of the rack, the behaviour is similar to a free overfall, requiring some distance to change the streamlines, and to reach the maximum values of the C_{qH}. In each rack slope, the maximum values seem to obtain similar results with the different inlet flows tested. The rack slope tends to modify the maximum value. Hence, bigger rack slopes tend to obtain smaller maximum C_{qH} values. After the maximum, the discharge coefficient tends to reduce with the decreasing of the water depth over the rack. Differences to the empirical formulae proposal by García (2016), corrected by the factor shown in Table 8, are due to the author considering that the energy remains constant along the rack.

DISCUSSION

Intake systems are used in stepped streams to obtain water, minimizing the sediment collection. The basic idea may be extrapolated to semiarid regions, in which the lack of water is a problem to deal with.

Boundary layer separation and high turbulence appear in bottom intake systems. In addition, the water depths in some sections of the rack and the spacing between bars make it difficult to use intrusive instrumentation.

Numerical simulations can help in the choice of the right intake system design but prior to this they should be compared with experimental and field data.

In this paper, the accuracy of ANSYS CFX to solve an intake system has been tested. Simulations have been compared with laboratory data, obtaining good agreement in several parameters. This study complements previous laboratory works (Noseda 1956a, 1956b; Brunella *et al.* 2003; Righetti & Lanzoni 2008; Castillo *et al.* 2014b, 2016, 2017b; García 2016) in bottom intake systems with T-shaped bars disposed longitudinally.

From the two classical assumptions shown in Table 1, numerical results show that the energy level is not constant along the rack. The energy level is somewhere between both simplifications, closer to being parallel to the rack plane than to the horizontal energy level (see Table 8).

According to different authors (see Figure 2), the rack length required to collect a desirable flow may vary up to two-fold. This range of possible values generates uncertainty in designers. In these situations, numerical models previously validated may reduce the lack of confidence during the design of intake systems and complement the laboratory studies.

Numerical simulations require a mesh sensitivity analysis. With mesh sizes of 0.004 m (around 1/3 of the spacing between bars in this case), the results are independent of the mesh size. Smaller mesh sizes would require more computational effort without remarkable differences in the results. Larger mesh sizes tend to obtain flow profiles below the laboratory measurements.

Regarding the choice of turbulence models, three different turbulence models have been considered. The results obtained are almost the same, with no significant differences between them. Based on previous studies in free-falling jets, the SST turbulence model was selected.

Once the sensitivity analysis was done, different comparisons were been considered. Regarding the flow profiles over the rack, the results are in agreement with the laboratory measurements for all the cases analysed. In the same way, the maximum wetted rack lengths over the bars and over the spacing diverge around 1% from the laboratory measurements. The results obtained for the water collected along the rack are also quite similar.

Finally, the sinus of the angle of the velocity vector of water collected with the rack plane has been considered as a discharge coefficient along the rack. The results are in agreement with previous studies published by Righetti & Lanzoni (2008) and by García (2016).

CONCLUSIONS

The results obtained with ANSYS CFX offered good agreement with the laboratory measurements and the empirical formulae (differences smaller than 1%). In this way, simulations can be used to complement laboratory and empirical data, allowing a better design to be obtained.

Numerical results are sensitive to the mesh size considered. In this way, the mesh size needs to be reduced until no significant differences are obtained between the results.

The extensive typology of bar shapes and settings of bottom intake systems do not allow to directly extrapolate results to other rack types. To reach accurate numerical results, several laboratory data are required, such as the water depth at the inlet channel or the flow profile along the rack.

With the aim of improving the design of bottom intake systems, it would be necessary to provide advances in the knowledge and characteristics of the flow through the rack. More experimental studies, both in physical models and prototypes, are necessary in characterizing the flow, combining measurements of pressures, velocities and flow profiles in T-shape and other types of bars.

ACKNOWLEDGEMENTS

The authors are grateful for the financial support received from the Seneca Foundation of Región de Murcia (Spain) through the project 'Optimización de los sistemas de captación de fondo para zonas semiáridas y caudales con alto contenido de sedimentos. Definición de los parámetros de diseño', reference: 19490/PI/14.

REFERENCES

Ahmad, Z. & Mittal, M. K. 2003 Hydraulic design of trench weir on Dabka river. *Water and Energy International* **60** (4), 28–37.

ANSYS Inc. 2015 ANSYS CFX. Solver Theory Guide. Release 16.2.

Bayon, A., Valero, D., García-Bartual, R., Vallés-Morán, F. J. & López-Jiménez, P. A. 2016 Performance assessment of OpenFOAM and FLOW-3D in the numerical modeling of a low Reynolds number hydraulic jump. *Journal of Environmental Modelling & Software* **80**, 322–335. doi: http://dx.doi.org/10.1016/j.envsoft.2016.02.018.

Bouvard, M. 1953 Debit d'une grille par en dessous (Discharge passing through a bottom grid). *La Houille Blanche* **2**, 290–291 (in French). doi: http://dx.doi.org/10.1051/lhb/1953027.

Bouvard, M. 1992 *Mobile Barrages and Intakes on Sediment Transporting Rivers*. IAHR Monograph Series, A. A. Balkema, Rotterdam, The Netherlands.

Brunella, S., Hager, W. & Minor, H. 2003 Hydraulics of bottom rack intake. *Journal of Hydraulic Engineering* **129** (1), 2–10. doi: http://dx.doi.org/10.1061/(ASCE)0733-9429(2003)129:1(2).

Castillo, L. G. & Carrillo, J. M. 2017 Comparison of methods to estimate the scour downstream of a ski jump. *International Journal of Multiphase Flow* **92**, 171–180. doi: https://doi.org/10.1016/j.ijmultiphaseflow.2017.03.006.

Castillo, L. G. & Lima, P. 2010 Análisis del dimensionamiento de la longitud de reja de una captación de fondo (Analysis of the dimensioning of the rack length of a bottom intake). In: *Proceedings of the XXIV Congreso Latinoamericano de Hidráulica*, Punta del Este, Uruguay (in Spanish).

Castillo, L. G., Carrillo, J. M. & Sordo-Ward, A. 2014a Simulation of overflow nappe impingement jets. *Journal of Hydroinformatics* **26** (4), 583–607. doi: 10.2166/hydro.2014.109.

Castillo, L. G., García, J. T. & Carrillo, J. M. 2014b Experimental measurements of flow and sediment transport through bottom racks – influence of gravels sizes on the rack. In: *Proceedings of the 7th International Conference on Fluvial Hydraulics, RIVER FLOW 2014*, Lausanne, Switzerland, pp. 2165–2172. doi: 10.1201/b17133-290.

Castillo, L. G., Carrillo, J. M. & Álvarez, M. A. 2015 Complementary methods for determining the sedimentation and flushing in a reservoir. *Journal of Hydraulic Engineering* **141** (11), 1–10. doi: http://doi.org/10.1061/(ASCE)HY.1943-7900.0001050.

Castillo, L. G., García, J. T. & Carrillo, J. M. 2016 Experimental and numerical study of bottom rack occlusion by flow with gravel-sized sediment. Application to ephemeral streams in semi-arid regions. *Water* **8** (4), 166. doi: 10.3390/w8040166.

Castillo, L. G., Carrillo, J. M. & Bombardelli, F. A. 2017a Distribution of mean flow and turbulence statistics in plunge pools. *Journal of Hydroinformatics* **19** (2), 173–190. doi: 10.2166/hydro.2016.044.

Castillo, L. G., García, J. T. & Carrillo, J. M. 2017b Influence of rack slope and approaching conditions in bottom intake systems. *Water* **9** (1), 65. doi: 10.3390/w9010065.

Chaguinov, G. N. 1937 *Prise d'eau du type tyrolien (Tyrolean Water Intake)*. *Thesis*, Moscow (in French).

Chanson, H. & Gualtieri, C. 2008 Similitude and scale effects of air entrainment in hydraulic jumps. *Journal of Hydraulic Research* **46** (1), 35–44.

Dagan, G. 1963 Notes sur le calcul hydraulique des grilles par-dessous (Notes on the hydraulic design of bottom-type intake screens). *La Houille Blanche* **18** (1), 59–65 (in French).

De Marchi, G. 1947 Profili longitudinali della superficie libera delle correnti permanenti lineari con portata progressivamente crescente o progressivamente decrescente

entro canali di sezione constant (Longitudinal profiles of the free surface of steady flows with progressively increasing or progressively decreasing flow rates within constant section channels). In: *Ricerca Scientifica e Ricostruzione*, February–March, pp. 203–208 (in Italian).

Drobir, H. 1981 Entwurf von Wasserfassungen im Hochgebirge (Design of water intakes inmountains rivers). *Österreichische Wasserwirtschaft* **11** (12), 243–253 (in German).

Drobir, H., Kienberger, V. & Krouzecky, N. 1999 The wetted rack length of the Tyrolean weir. In: *Proceedings of the IAHR-28th Congress*, Graz, Austria.

Frank, J. & Von Obering, E. 1956 Hydraulische Untersuchungen für das Tiroler Wehr (Hydraulic research for the Tyrolean intake). *Der Bauingenieur* **31** (3), 96–101 (in German).

García, J. T. 2016 *Estudio experimental y numérico de los sistemas de captación de fondo (Experimental and Numerical Study of the Bottom Intake Systems)*. PhD Thesis, Universidad Politécnica de Cartagena, Cartagena, Spain (in Spanish).

Garot, F. 1939 De Watervang met liggend rooster (The intake with lying rack). *De Ingenieur in Nederlandsch Indie* **6** (7), 115–132 (in Dutch).

Gherardelli, S. 1956 Sul calcolo idraulico delle griglie di fondo (On the hydraulic calculation of the bottom racks). *Energia Elettrica*, 1347 (in Italian).

Ghosh, S. & Ahmad, Z. 2006 Characteristics of flow over bottom racks. *Water and Energy International* **63** (2), 47–55.

Henderson, F. M. N. 1966 *Open Channel Flow.* MacMillan, New York, USA.

Krochin, S. 1978 *Diseño Hidráulico (Hydraulic Design),* 2nd edn. EPN, Quito, Ecuador, pp. 97–106 (in Spanish).

Kumar, S., Ahmad, Z., Kothyari, U. C. & Mittal, M. K. 2010 Discharge characteristics of a trench weir. *Flow Measurement and Instrumentation* **21** (2), 80–87. doi:10.1016/j.flowmeasinst.2010.01.002.

Kuntzmann, J. & Bouvard, M. 1954 Étude théorique des grilles de prises d'eau du type en dessous (Theoretical study of bottom type water intake grids). *La Houille Blanche* **5**, 569–574 (in French). doi:http://dx.doi.org/10.1051/lhb/1954049.

Launder, B. E. & Sharma, B. I. 1972 Application of the energy-dissipation model of turbulence to the calculation of flow near a spinning disc. *Letters in Heat and Mass Transfer* **1** (2), 131–138.

Menter, F. R. 1994 Two-equation eddy-viscosity turbulence models for engineering applications. *AIAA Journal* **32** (8), 1598–1605.

Mostkow, M. 1957 Sur le calcul des grilles de prise d'eau (Theoretical study of bottom type water intake). *La Houille Blanche* **12** (4), 570–580 (in French).

Nakagawa, H. 1969 On hydraulic performance of bottom diversion works. *Bulletin of Disaster Prevention Research Institute* **18** (3), 29–48.

Noseda, G. 1956a Correnti permanenti con portata progressivamente decrescente, defluenti su griglie di fondo (Steady flow with progressively decreasing flow rate, flowing on bottom racks). *L'Energia Elettrica* **33** (1), 41–51 (in Italian).

Noseda, G. 1956b Correnti permanenti con portata progressivamente decrescente, defluenti su griglie di fondo (Steady flow with progressively decreasing flow rate, flowing on bottom racks). *L'Energia Elettrica* **33** (6), 565–588 (in Italian).

Orth, J., Chardonnet, E. & Meynardi, G. 1954 Étude de grilles pour prises d'eau du type en-dessous (Study of bottom type water intake grids). *La Houille Blanche* **9** (6), 343–351 (in French).

Ract-Madoux, M., Bouvard, M., Molbert, J. & Zumstein, J. 1955 Quelques réalisations récentes de prises en-dessous à haute altitude en Savoie (Recently built high altitude bottom intakes). *La Houille Blanche* **10** (6), 852–878 (in French).

Raudkivi, A. J. 1993 *Hydraulic Structures Design Manual.* IAHR Monograph, Balkema, Rotterdam, pp. 92–105.

Righetti, M. & Lanzoni, S. 2008 Experimental study of the flow field over bottom intake racks. *Journal of Hydraulic Engineering* **134** (1), 15–22.

Righetti, M., Rigon, R. & Lanzoni, S. 2000 Indagine sperimentale del deflusso attraverso una griglia di fondo a barre longitudinali (Experimental research of the flow through a bottom rack with longitudinal bars). In: *Proceedings of the XXVII Convegno di Idraulica e Costruzioni Idrauliche*, Vol. 3, Genova, Italy pp. 112–119 (in Italian).

USACE (U.S. Army Corps of Engineers' River Naysays System) 2016 *HEC-RAS River Analysis System. Hydraulic Reference Manual*. Version 5.0.

Vargas, V. 1998 Tomas de fondo (Intake systems). In: *Proceedings of the XVIII Congreso Latinoamericano de Hidráulica*, Oaxaca, Mexico (in Spanish).

White, J. K., Charlton, J. A. & Ramsay, C. A. W. 1972 On the design of bottom intakes for diverting stream flows. *Proceedings of the Institution of Civil Engineers* **51**, 337–345.

Wilcox, D. C. 2006 *Turbulence Modeling for CFD*, 3rd edn. DCW Industries, Inc., La Canada, California, USA.

Yakhot, V. & Smith, L. M. 1992 The renormalization group, the ε-expansion and derivation of turbulence models. *Journal of Scientific Computing* **7** (1), 35–61.

First received 10 January 2017; accepted in revised form 12 July 2017. Available online 12 September 2017